

## Supporting Information's for

# Acyl amide-Functionalized and Water-Stable Iron-Based MOF For Rapid and Selective Dye Removal

Hosein Ghasempour<sup>a</sup>, Farnoosh Zarekarizi<sup>a</sup>, Ali Morsali<sup>a\*</sup>

<sup>a</sup> Department of Chemistry, Faculty of Sciences, Tarbiat Modares University, P.O. Box 14117-13116, Tehran, Islamic Republic of Iran

\* Corresponding Author, Morsali\_a@modares.ac.ir

## 1. Reagents and Apparatus.

All used chemical reagents including organic dyes and initial reagent for linker and MOF fabrication, were prepared from commercial resources and were used without any purification.

Philips instrument with X'pert diffractometer under radiation of monochromated Cu K $\alpha$  was applied to measure the Powder X-ray diffraction (PXRD) patterns. The volumetric isotherms of N<sub>2</sub> sorption/desorption were collected under 77 K with a TriStar II 3020 equipment from Micromeritics Instrument Corporation (liquid nitrogen bath applied to Temperature controlling and  $V_t$  was calculated at  $P/P_0 = 0.3$ ). UV–Vis spectra are performed on a Varian Cary-50 spectrophotometer equipped with a single-beam facility with a spectral resolution of 0.2 nm. Fourier transform infrared (FT-IR) diagrams were collected in the range of 400-4000 cm<sup>-1</sup> using a Bruker Tensor 27FTIR instrument through KBr tablet. A Bruker Avance DPX of 250 MHz (5.8 T) NMR spectrometer was used to collect the <sup>1</sup>H NMR spectra. BesTec spectrometer X-ray photoelectron spectroscopy (XPS) was used for XPS analyses under ultrahigh vacuum. The 284.9 eV peak of C 1s was used for the binding energy calibration.

## 2. Equations

*Removal efficiency.* The removal percentage ( $R \%$ ) and adsorption capacity ( $Q_e$   $\text{mg.g}^{-1}$ ) of adsorbent at a special period of time were obtained from equations 1 and 2:

$$R \% = ((C_0 - C_e) / C_0) \times 100 \quad (1), \quad Q_e = (C_0 - C_e) V / m \quad (2)$$

where  $m$ ,  $V$ ,  $C_0$  and  $C_e$  are related to the mass of adsorbent (mg), the volume of dye solution (mL), initial and equilibrium concentrations of dyes ( $\text{mg.L}^{-1}$ ), respectively.

*Langmuir model.* The equation 3 below displays the linear formula of Langmuir isotherm;

$$C_e / q_e = 1 / (K_1 \cdot q_m) + C_e / q_m \quad (3)$$

where  $q_m$  ( $\text{mg.g}^{-1}$ ) and  $K_1$  ( $\text{L.mg}^{-1}$ ) are the maximum adsorption capacity and the Langmuir adsorption rate constant (related to dependence of adsorbent and adsorbate), respectively.

*Freundlich model.* Freundlich isotherm defines a non-ideal and reversible adsorption that is ascribed to multiple-layer adsorption on heterogeneous surface.

This model can be determined by equation 4:

$$\log q_e = \log K_F + 1/n \log C_e \quad (4)$$

where  $K_F$  is Freundlich constants and  $1/n$  is adsorption intensity which specifies the adsorption desirability.

*Kinetic equations.* The equation 5 expresses the pseudo-first-order kinetic equation:

$$\log(q_e - q_t) = \log q_e - k_1 t / 2.303 \quad (5)$$

and the equation 6 shows the linear form pseudo-second-order kinetic model;

$$t/q_t = 1/k_2 q_e^2 + t/q_e \quad (6)$$

where  $q_t$  is the stationary binding capacity ( $\text{mg.g}^{-1}$ ) at various times  $t$  (min),  $q_e$  is the theoretical adsorption capacity for pseudo-first-order kinetics ( $\text{mg.g}^{-1}$ ), and  $k_1$  is the rate constant of pseudo-first-order kinetic model [ $\text{g.mg}^{-1}.\text{min}^{-1}$ ] and  $k_2$  is the rate constant of pseudo-second-order kinetic model [ $\text{g.mg}^{-1}.\text{min}^{-1}$ ].

Adsorption procedure is a multi-step process including the transmission of guest molecules from the solution media near the host surface followed by diffusing to the apertures of host pores (kinetic determinative step) is favored kinetic model when the pseudo first/second order kinetic models are not able to describe the diffusion mechanism. The subsequent equation states the Intraparticle diffusion model:

$$q_t = k_p t^{1/2} + I \quad (7)$$

where  $k_p$  ( $\text{mg}\cdot\text{g}^{-1}\cdot\text{min}^{-0.5}$ ) and  $I$  here are the diffusion rate constant and the intercept, respectively.

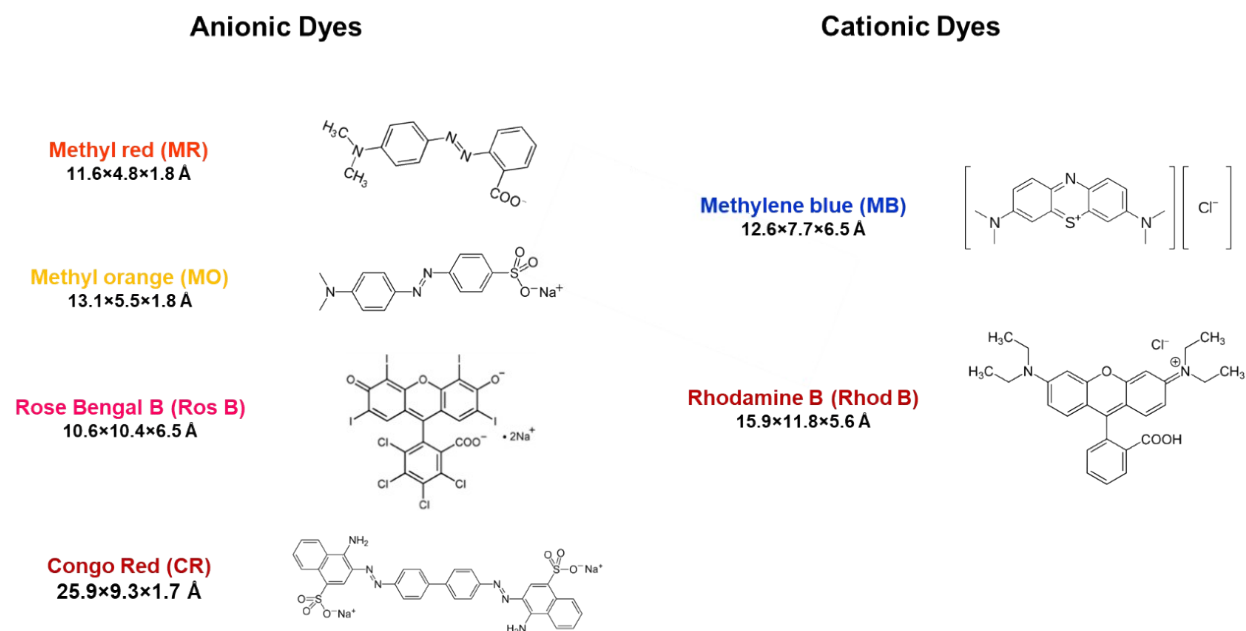


**Figure S1.** Studied organic dyes strut.

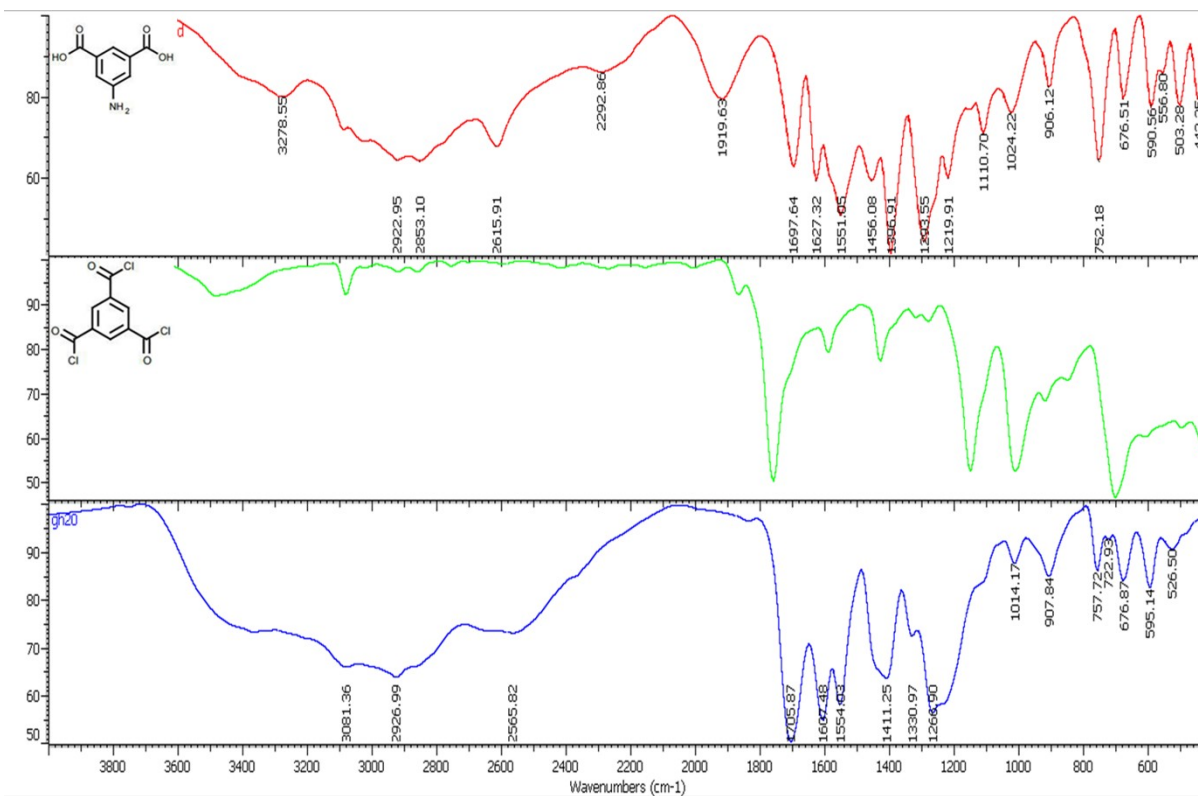


**Figure S2.** FT-IR of H<sub>6</sub>TPBTM linker (blue) compared to initial reactants. Selected IR peaks (KBr, cm<sup>-1</sup>): 1708, 1606, 1550, 1426, 1332, 1277, 1226, 1128, 1001, 952, 908, 757, 720, 667, 591.

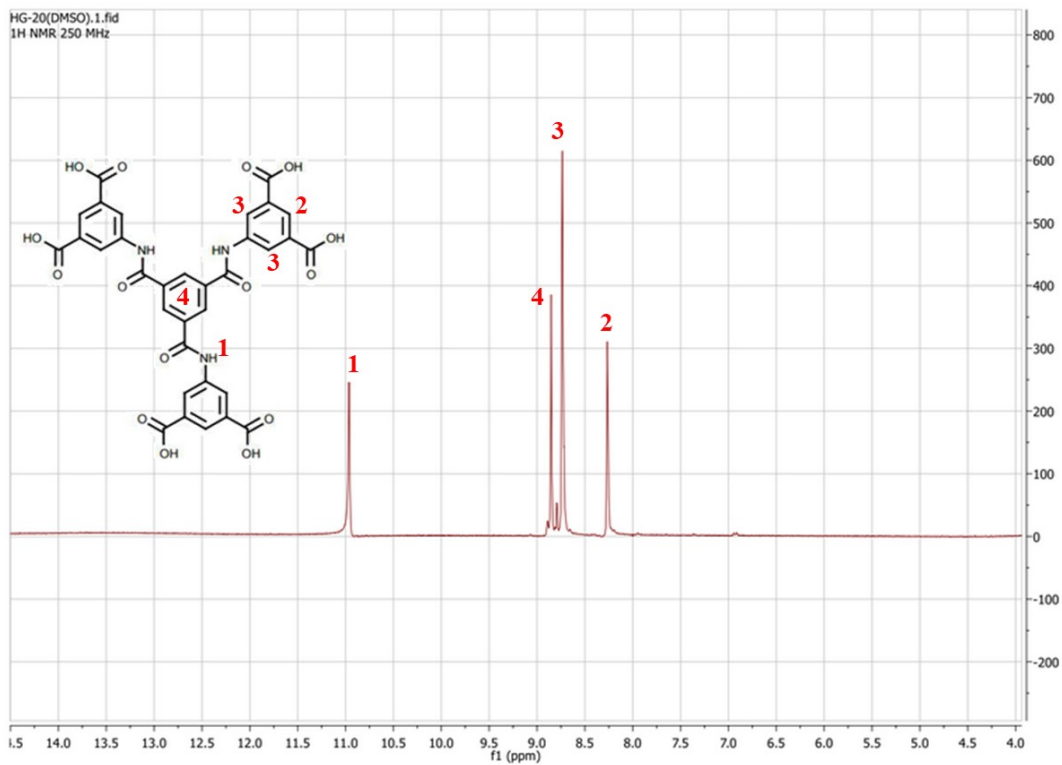


**Figure S3.** <sup>1</sup>H-NMR of H<sub>6</sub>TPBTM linker, (250 MHz, DMSO-*d*<sub>6</sub>,  $\delta$  ppm): 13.67 (wide peak, carboxylic acid 1H), 10.97 (s, amidic 3H), 8.86 (s, Aromatic 3H), 8.72 (d, Aromatic 6H), 8.25 (t, Aromatic 3H).

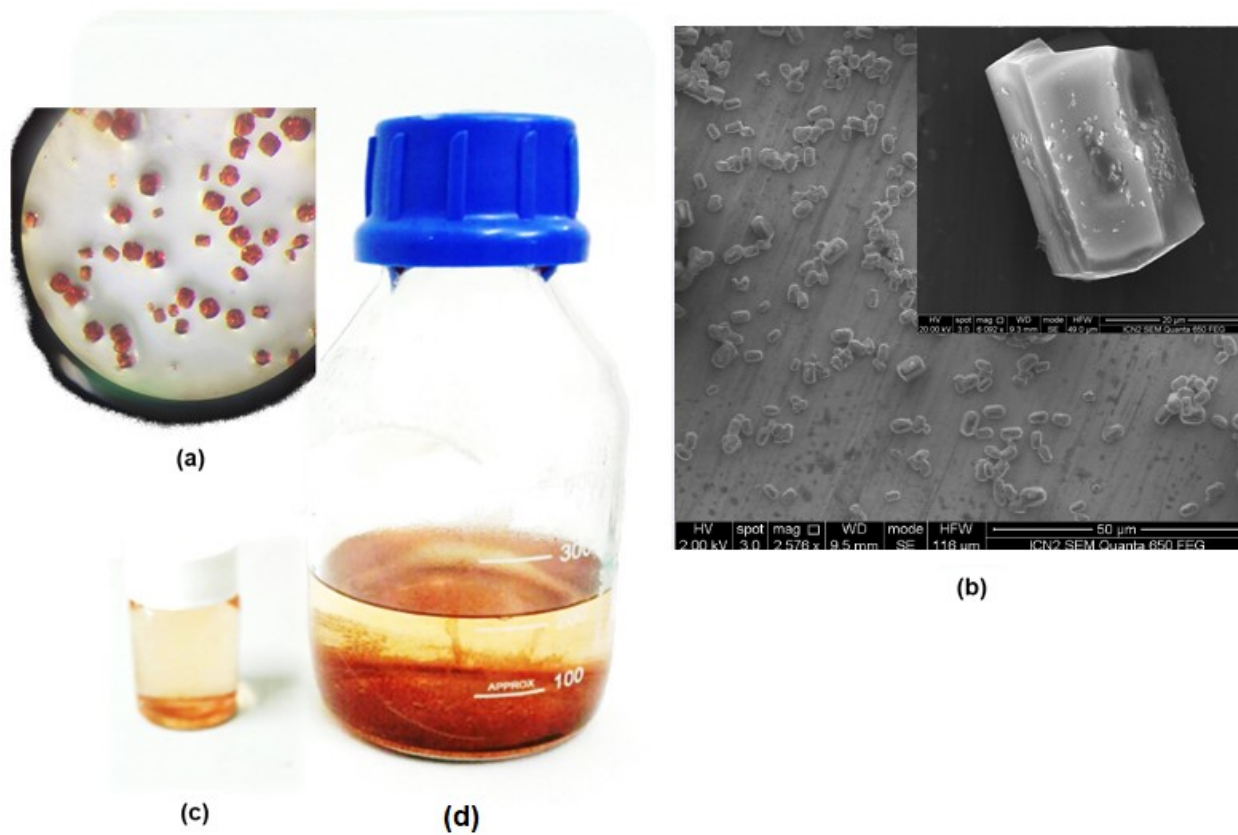


**Figure S4.** Photograph (a) and SEM (b) images of Fe-MOF crystals. Milligram (c) and gram scale (d) synthesis of Fe-MOF. Selected IR (KBr,  $\text{cm}^{-1}$ ): 1663, 1621, 1577, 1424, 1382, 1329, 1242, 1105, 1017, 778, 713, 592.



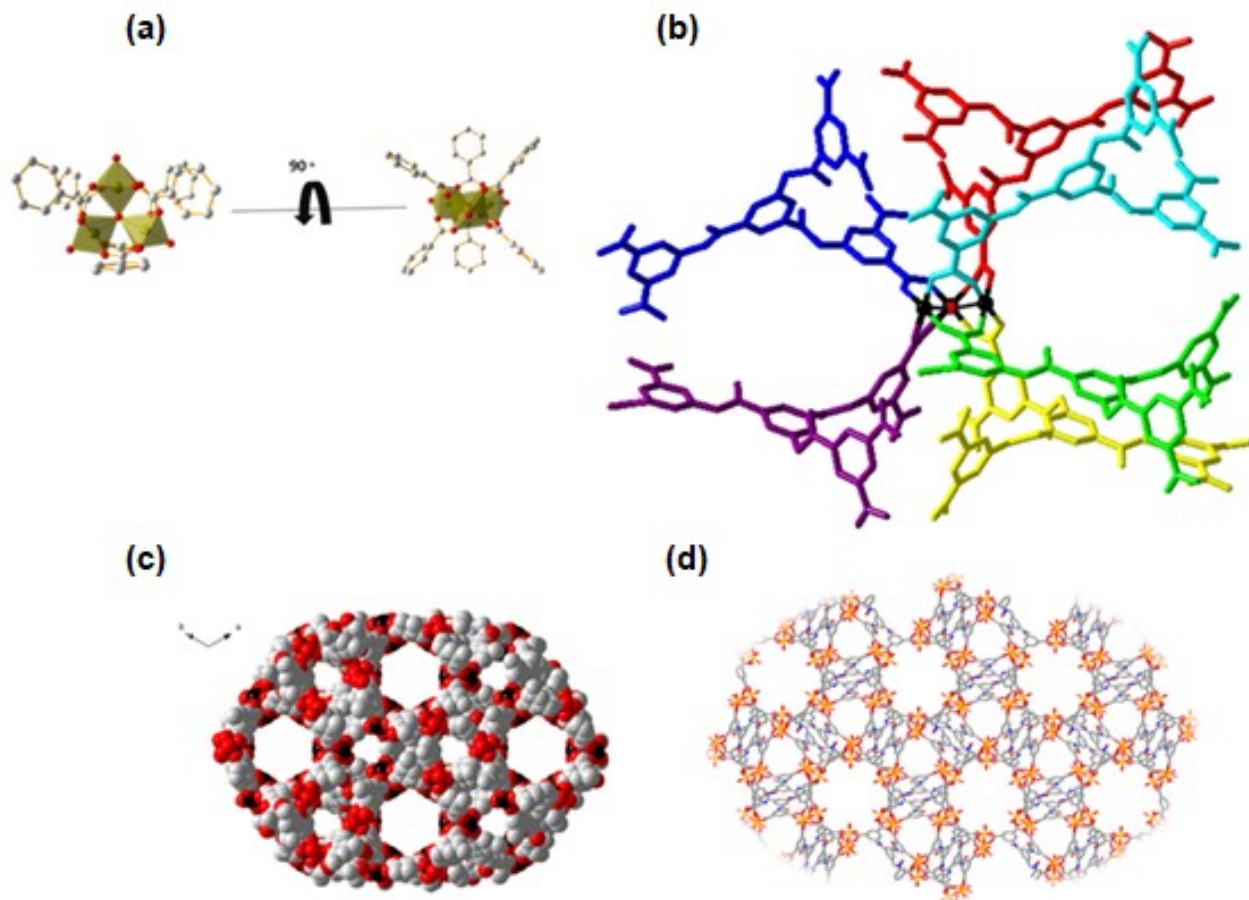


**Figure S5.** The coordination environment of metal cluster (a), structural unit of a metal cluster with six connected ligands (b), the Space-fill (c) and Wireframe (d) representation of stacked structure of Fe-MOF along crystallographic c axis.

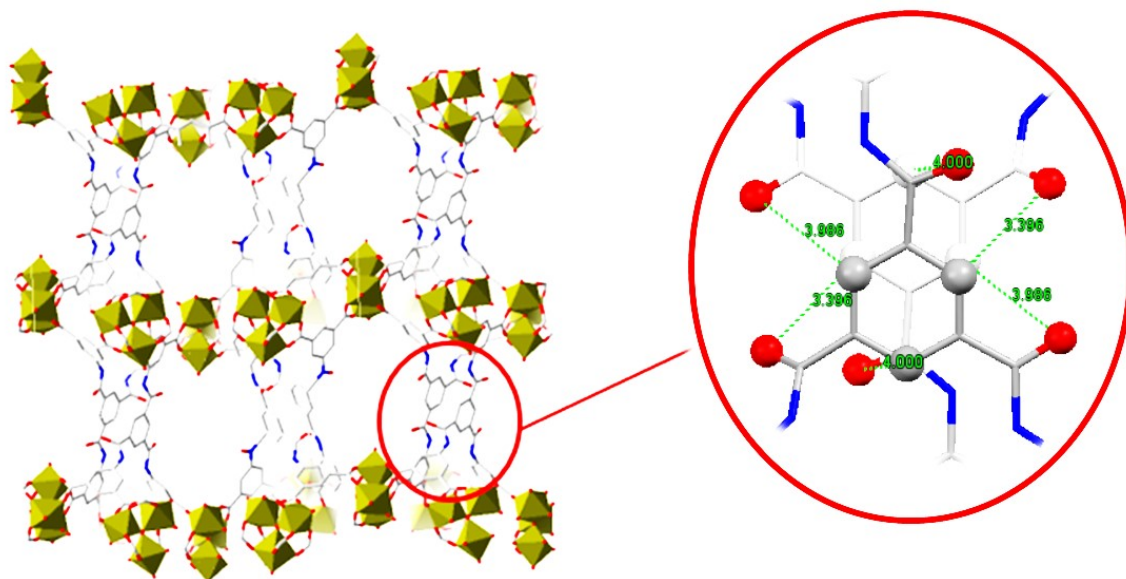


**Figure S6.** A fragment of Fe-MOF structure as a pillar layered MOF (left), two parallel ligands core act as a pillaring strut (right).

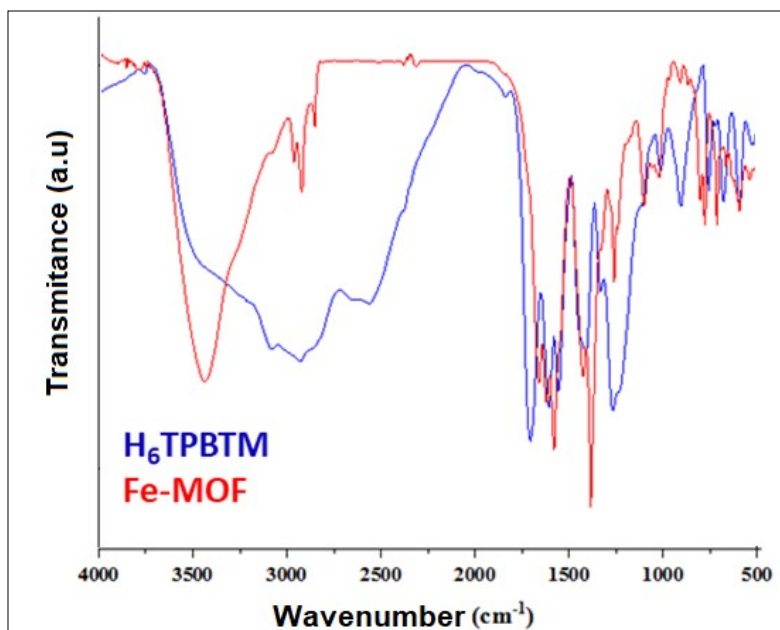


**Figure S7.** FT-IR spectra of H<sub>6</sub>TPBTM linker (blue) and Fe-MOF (red).

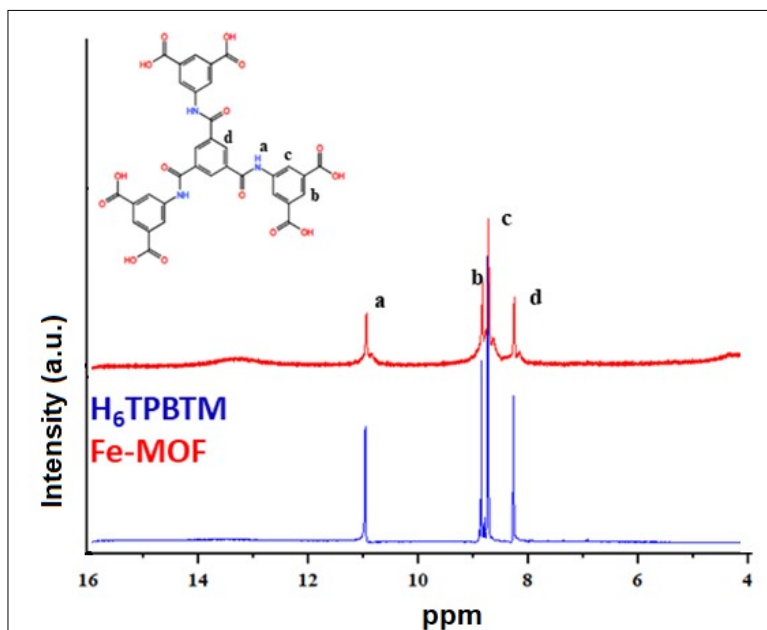


**Figure S8.** <sup>1</sup>H-NMR of H<sub>6</sub>TPBTM linker (blue) and digested Fe-MOF crystals in D<sub>2</sub>SO<sub>4</sub>(red).

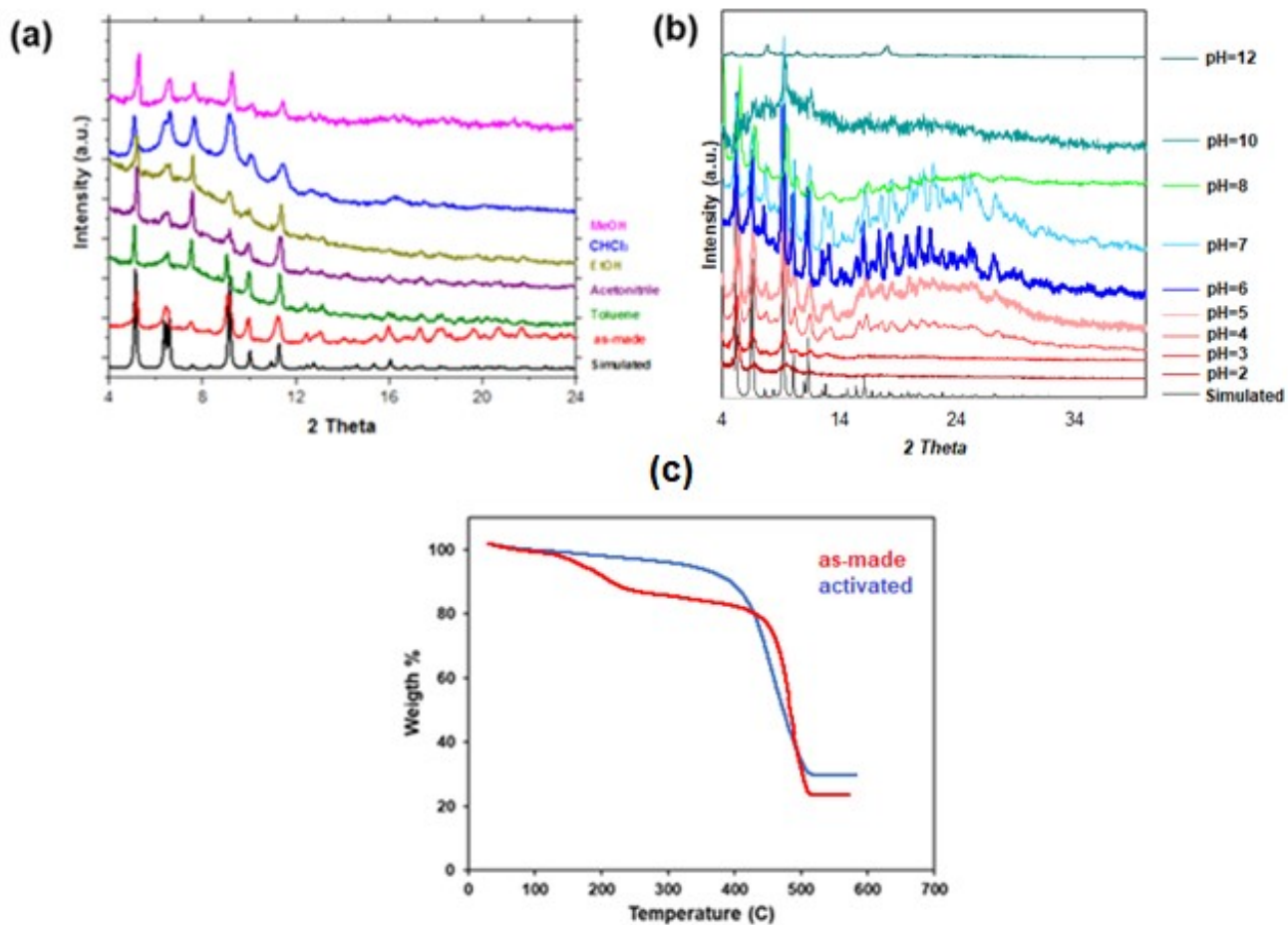


**Figure S9.** PXRD diagram of immersed crystals of Fe-MOF in diverse organic solvents (a) and aqueous solution with different pH (b) in comparison with simulated pattern. TGA curve of as-made and activated Fe-MOF (c).

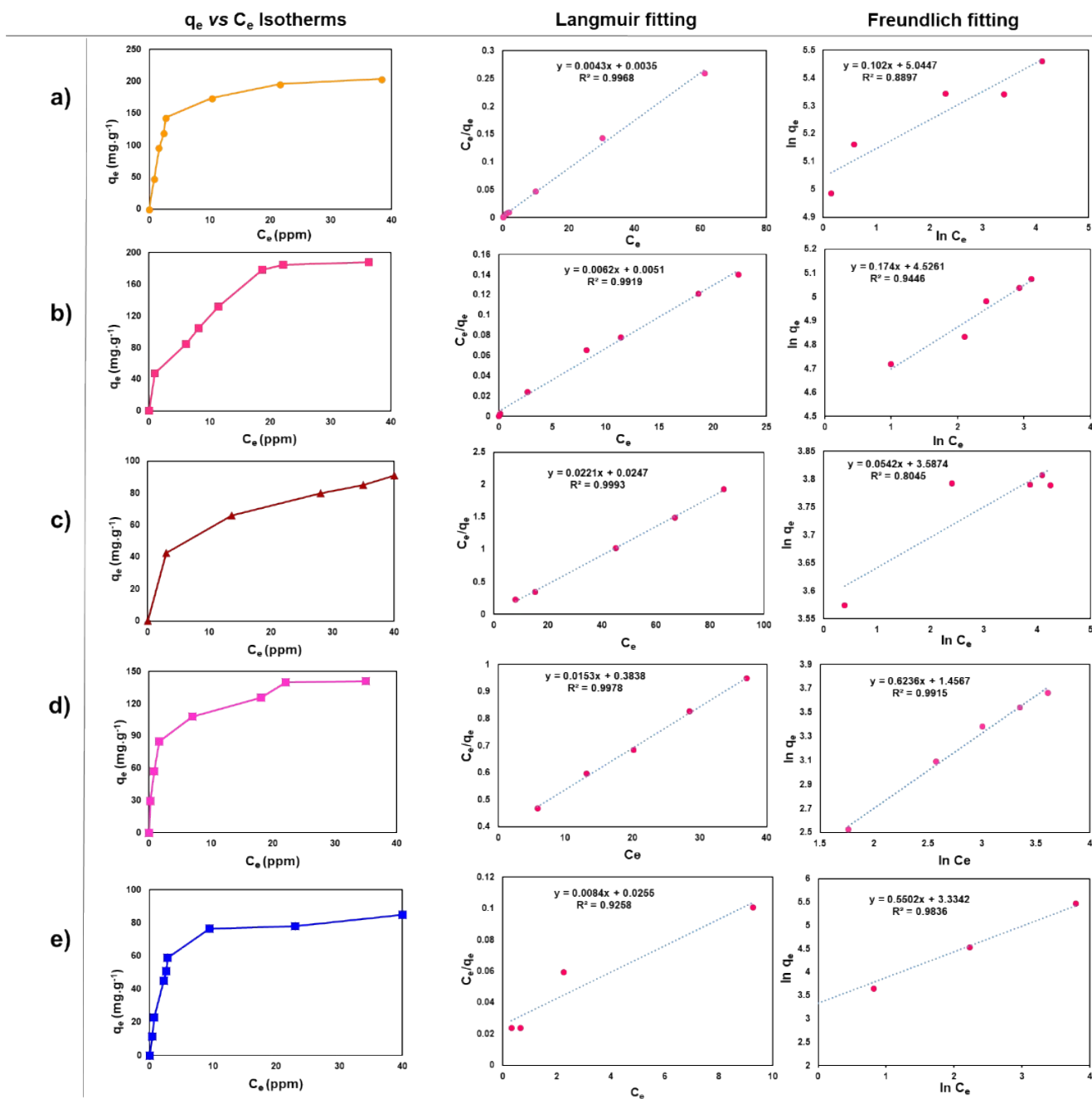


**Figure S10.** The  $q_e$  vs  $C_e$  isotherms, Langmuir and Freundlich fitting of experimental adsorption of MO (a), MR (b), CR, Ros B (d) and MB (e) by Fe-MOF adsorbent.

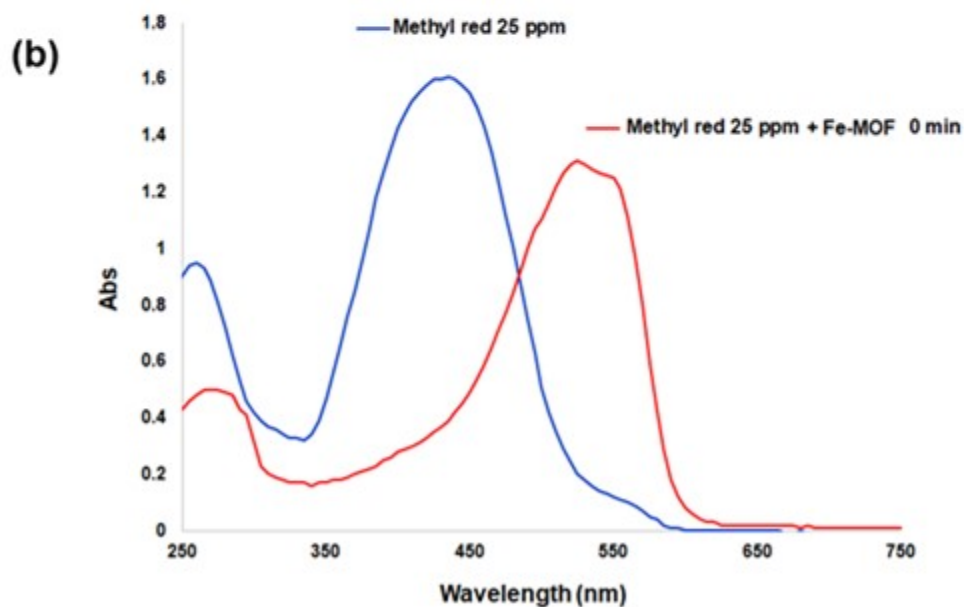


**Figure S11.** pH dependent interplay between anionic and natural form of MR dye and corresponding solution color (a), red-shift of MR absorbance band in UV-vis spectra in the presence of Fe-MOF (b).

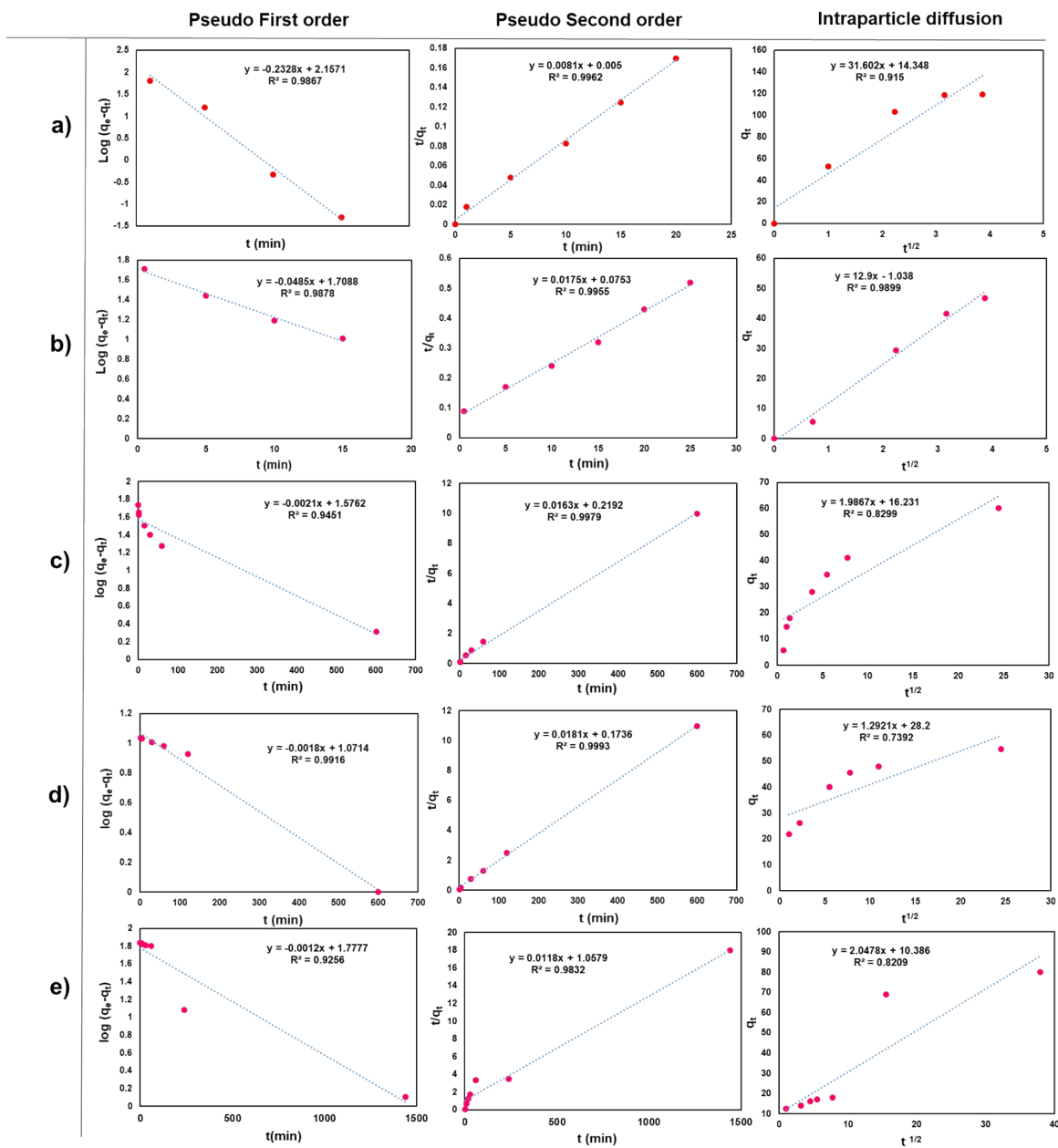
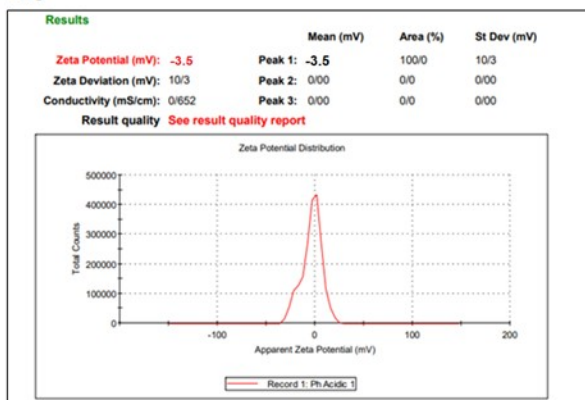
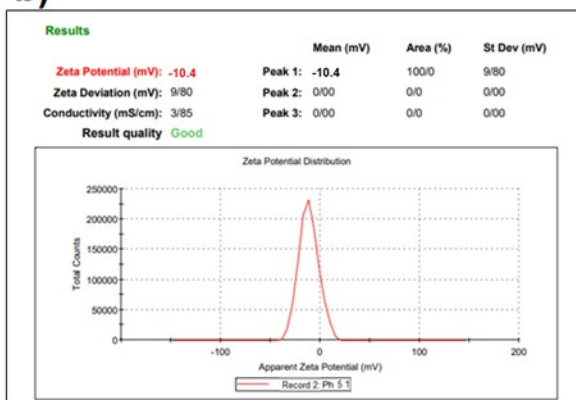


**Figure S12.** Fitted experimental kinetic adsorption data of MO (a), MR (b), (CR), Ros B (d) and MB (e) by Fe-MOF adsorbent with pseudo-first-order, pseudo-second-order and intraparticle diffusion model.

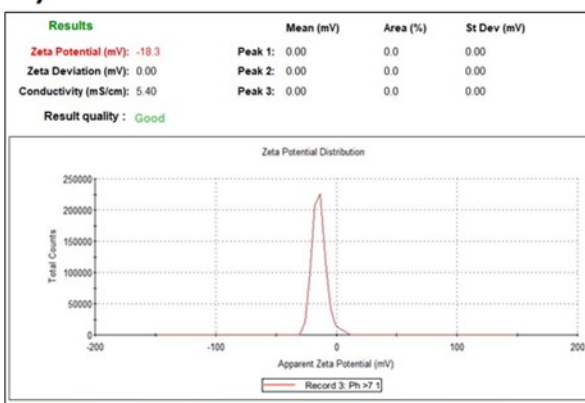
a)



b)



c)



d)

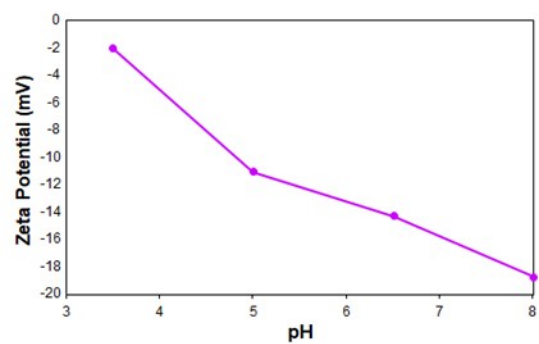
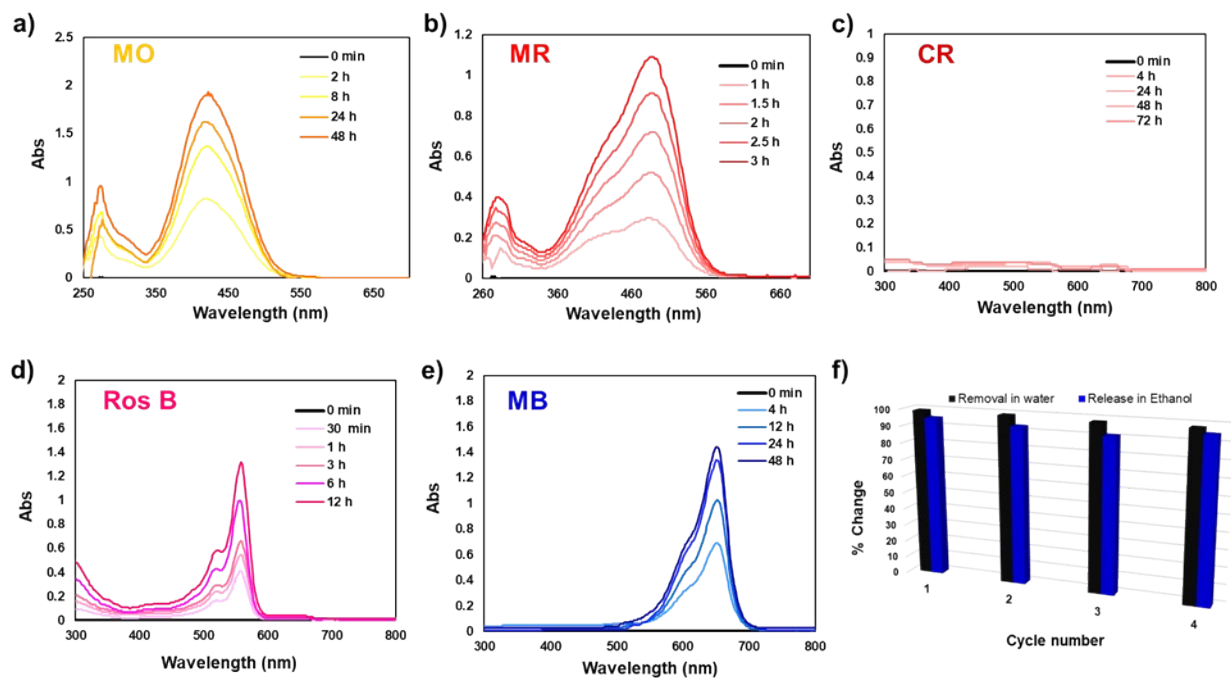


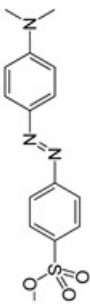
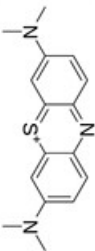
Figure S13. Zeta Potential distribution of Fe-MOF in low, normal and high pH media (a-c) and Zeta potential vs pH curve.





**Figure S14.** UV-vis profiles of releasing adsorbed dyes to ethanolic solution passing time; MO (a), MR (b), CR (c), Ros B (d), and MB (e). Removal and release of MO by Fe-MOF for four cycles (f).

**Table S1.** Comparison of Fe-MOF adsorption capacity toward MO and MB with some of famous MOFs.

Dye	Adsorbent MOFs	Adsorption Capacity (mg.g <sup>-1</sup> )	Ref.
<b>MO</b> 	ZIF-8	75	1
	ZIF-67	201	2
	MIL-100(Fe)	1045	3
	UiO-66	39	4
	UiO-66-NH <sub>2</sub>	28	
	UiO-66-NO <sub>2</sub>	142	5
	MIL-53	57	6
	MIL-101	114	
	NH <sub>2</sub> -MIL-101	188	7
	MOF-74	239	8
	MIL-100-Cr	211	3
	<b>Fe-MOF</b>	<b>232</b>	<b>This study</b>
<b>MB</b> 	ZIF-8	24	9
	MIL-101	10	10
	Fe <sub>3</sub> O <sub>4</sub> @MIL-100	73	11
	MOF-74	370	8
	HKUST-1	5	12
	Cu-BTC	143	13
	MOF-5	107	14
	UiO-66	90	4
	UiO-66-NH <sub>2</sub>	96	
	UiO-66-NO <sub>2</sub>	41	5
	<b>Fe-MOF</b>	<b>120</b>	<b>This study</b>

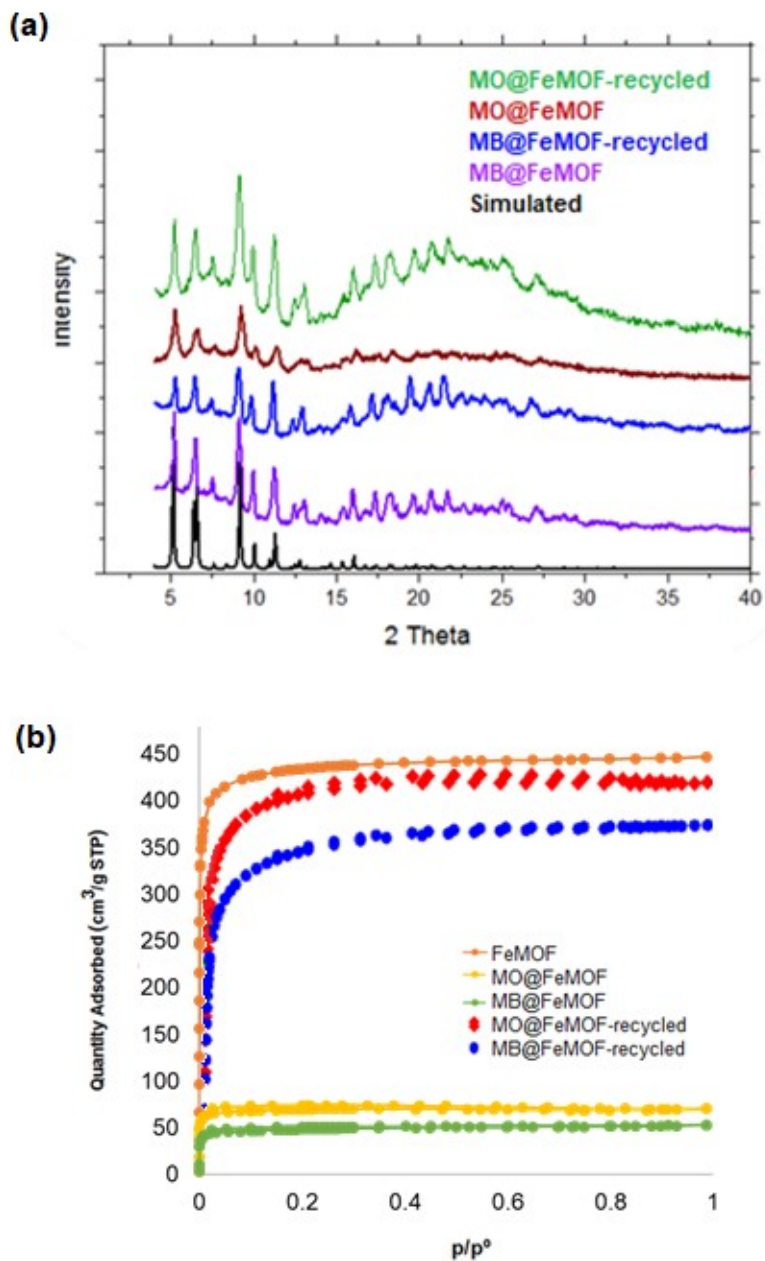


**Figure S15.** (a) PXRD diagram of MO and MB adsorbed/desorbed crystals compared to simulated PXRD from crystallographic data. (b) N<sub>2</sub> sorption isotherm of MO and MB adsorbed/desorbed crystals compared to fresh active Fe-MOF.

## References

1. Y. Ding, Y. Xu, B. Ding, Z. Li, F. Xie, F. Zhang, H. Wang, J. Liu and X. Wang, *Colloids Surfaces A: Physicochemical Engineering Aspects*, 2017, 520, 661-667.
2. D.O. Sulistiono, R. Ediati, AIP Publishing LLC, 2021, 020067.
3. M. Tong, D. Liu, Q. Yang, S. Devautour-Vinot, G. Maurin and C. Zhong, *Journal of Materials Chemistry A*, 2013, 1, 8534-8537.
4. Q. Chen, Q. He, M. Lv, Y. Xu, H. Yang, X. Liu and F. Wei, *Applied Surface Science*, 2015, 327, 77-85.
5. H. T. Dinh, N. T. Tran and D. X. Trinh, *Journal of Analytical Methods in Chemistry*, 2021, 2021.
6. E. Haque, J. E. Lee, I. T. Jang, Y. K. Hwang, J.-S. Chang, J. Jegal and S. H. Jung, *Journal of Hazardous Materials*, 2010, 181, 535-542.
7. E. Haque, V. Lo, A. I. Minett, A. T. Harris and T. L. Church, *Journal of Materials Chemistry A*, 2014, 2, 193-203.
8. F. Ahmadijokani, R. Mohammadkhani, S. Ahmadipouya, A. Shokrgozar, M. Rezakazemi, H. Molavi, T. M. Aminabhavi and M. Arjmand, *Chemical Engineering Journal*, 2020, 399, 125346.
9. E. Santoso, R. Ediati, Z. Istiqomah, D. O. Sulistiono, R. E. Nugraha, Y. Kusumawati, H. Bahruji and D. Prasetyoko, *Microporous Mesoporous Materials*, 2021, 310, 110620.
10. T. Shen, J. Luo, S. Zhang and X. Luo, *Journal of Environmental Chemical Engineering*, 2015, 3, 1372-1383.
11. C.-F. Zhang, L.-G. Qiu, F. Ke, Y.-J. Zhu, Y.-P. Yuan, G.-S. Xu and X. Jiang, *Journal of Materials Chemistry A*, 2013, 1, 14329-14334.
12. S. Lin, Z. Song, G. Che, A. Ren, P. Li, C. Liu and J. Zhang, *Microporous and Mesoporous Materials*, 2014, 193, 27-34.
13. J. Hu, W. Dai, X. Yan., *Desalination Water Treatment*, 57 (2016) 4081-4089.
14. A. Fallah Shojaei, K. Tabatabaeian and M. Zebardast, *Scientia Iranica*, 2018, 25, 1323-1334.